IEEE Robotics and Automation Letters (RAL) paper presented at
2024 IEEE/RSJ International Conference on Intelligent Robots and Systems (IROS)
October 14-18, 2024. Abu Dhabi, UAE

Enhancing Maximum Stroke of Twisted String Actuators by Adjusting Twisting Ratio

Seungjoon Baek[1], *Student Member, IEEE*, JaeHyung Jang[2], and Jee-Hwan Ryu[2], *Senior Member, IEEE*

***Abstract*— In robotics, twisted string actuators (TSAs) have attracted considerable attention owing to their high gear ratio, flexibility, and simplicity. However, TSAs face challenges such as control issues, limited lifespan, and limited stroke. Among them, their practical use is hindered by a limited stroke due to overtwisting, leading to hysteresis, efficiency, and lifespan issues. To avoid overtwisting, TSAs are confined to a narrow stroke range, approximately 30% of the original string length. This study introduces an innovative approach to enhance TSA stroke without introducing overtwisting. The key lies in adjusting the ratio of overlap and individual twisting (ROI) to strategically use the string that possesses the capacity of twisting. The method capitalizes on the observation that the maximum strokes of two TSA twisting methods—twisted single string and twisted looped single string (TLS)—are approximately equal. This is attributed to the locking point induced by overlap twisting in TLS. To mathematically model this phenomenon, this study develops a novel kinematic model of TSA accounting for the locking point. Additionally, we propose an optimization process, achieving a maximum stroke of 53.44% of the original string length, significantly surpassing the conventional limitation of 30%. This enhancement is achieved without introducing overtwisting, thereby avoiding hysteresis.**

I. INTRODUCTION

Twisted string actuators (TSAs) are tendon-based actuators that operate by twisting a string to generate linear motion, thereby offering a unique actuation approach suitable for various applications in robotics. The working principle of TSAs involves the conversion of rotary motion into linear motion by the controlled twisting and untwisting of strings. TSAs are widely applicable in various fields, including soft robotics [1]–[3], wearable devices [4], [5], and medical instruments [6], [7]. The inherent compliance of the these actuators facilitates their safe interaction with humans, making them ideal for assistive devices and wearable exoskeletons. Moreover, TSAs are promising in haptic feedback systems [8], [9], providing a intuitive method for tactile sensations.

Manuscript received: January, 5, 2024; Revised: March, 27, 2024; Accepted: April, 22, 2024. This work was supported in part by the Agency for Defense Development under Grant 21-CM-GU-04 funded by the Ministry of National Defense (MND, Korea), in part by the Robot Industry Core Technology Development Program under Grant 20023294 funded by the Ministry of Trade, Industry and Energy (MOTIE, Korea), and in part by the National Research Foundation of Korea under Grant NRF-2020R1A2C200416915. (Seungjoon Baek and JaeHyung Jang are co-first authors.) (Corresponding author: Jee-Hwan Ryu.)

Seungjoon Baek is with the Robotics Program, Korea Advanced Institute of Science and Technology, Daejeon 34141, South Korea (e-mail: sjbaek12@kaist.ac.kr).

JaeHyung Jang and Jee-Hwan Ryu are with the Department of Civil and Environmental Engineering, Korea Advanced Institute of Science and Technology, Daejeon 34141, South Korea (e-mail: jhjang.kd@kaist.ac.kr; jhryu@kaist.ac.kr).

However, TSAs have several limitations, including control challenges, limited lifespan, and limited stroke. Among them, this study addresses the limited stroke originating from overtwisting, the twisting of TSA strings beyond a certain limit, causing the strings to twist nonuniformly and overlap indiscriminately with distortion [10]. Overtwisting presents a range of challenges, including hysteresis in the stroke and gear ratio [11], a reduced lifespan [10], [11], and diminished efficiency. Consequently, TSA usage has been confined to restricted strokes, typically 30% of the original string length. The constrained stroke of TSA imposes limitations on its application design, especially when constrained by conditions requiring a long original string length.

To address this challenge, the utilization of TSAs within the overtwisting range, involving a separator-based technique and the introduction of a mathematical model demonstrating the potential for replicating the actual stroke behavior during overtwisting, was proposed [10]. Additionally, TSAs were employed within the overtwisting interval through a training process aimed at configuring a uniform coil structure, resulting in a consistent output stroke behavior [11]. By implementing overtwisting, the two studies attained a maximum stroke of 81% and 70% for [10] and [11], respectively.

However, there are several drawbacks for overtwisting. In the overtwisting interval, hysteretic stroke and torque behavior inevitably occur because of their highly nonlinear behavior [11]. In other words, overtwisting makes it difficult to predict the behavior of TSAs. In addition, the coiling of the string involved in overtwisting requires a large motor torque [11]. Another drawback is that overtwisting accelerates the failure of strings (i.e., a decrease in lifespan) [10] because the strings are hard-squeezed and distorted during overtwisting. In addition, it is presumed that the method proposed in [10] will further limit the lifespan because of the separator.

This study presents an innovative approach for extending the maximum stroke of TSAs without introducing overtwisting. This extension was achieved through manipulating the ratio of overlap to individual twisting (ROI). First, we observed the following phenomenon: the maximum stroke achievable with a twisted single string (TSS) closely resembles that of a twisted looped single string (TLS). This similarity is intriguing because TSS employs one type of twisting, known as individual twisting (IT), whereas TLS employs two types of twisting, IT and overlap twisting (OT). This phenomenon can be explained by the impediment in the IT propagation, resulting in a decrease in the stroke. This impediment in the IT propagation is attributed to the occurrence of a locking point during the OT. Therefore, our

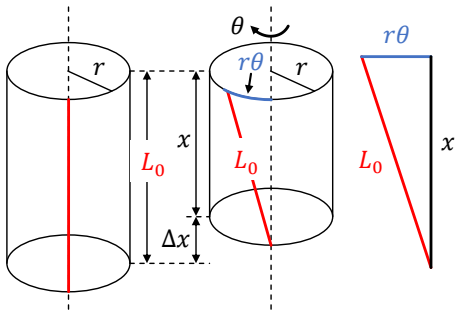

Fig. 1. Schematic representation of kinematic model of TSAs.

observation suggests that a greater amount of IT prior to encountering a locking point can yield an extended stroke, which constitutes the central concept of this research. To fully use the surplus capacity of IT within the string, thereby leading to an expansion in maximum stroke, the optimal ROI trajectory that maximizes this stroke capacity is created. The optimization of this trajectory relies on the proposed kinematic model of TSAs, considering the locking mechanism. To the best of our knowledge, this model and ROI optimization is the first in its kind. Our conducted verification confirmed the model's capability to accurately replicate the stroke behavior of TSAs across a range of ROIs. Significantly, the optimized ROI trajectory facilitated a maximum stroke of 53.44% of the original string length without introducing overtwisting, consequently leading to a hysteresis-free performance.

The remainder of this paper is organized as follows: Section II covers background on kinematics and overtwisting of TSAs. Section III analyzes the effect of locking on TLS. Section IV proposes a kinematic model of TSAs accounting for the locking and describes an optimization method. Section V provides the experimental results and discussion. Section VI concludes the paper.

II. Background: Kinematics and Overtwisting of TSAs

This section reviews the conventional kinematic model of TSAs, which determines output stroke x with respect to input motor rotation θ. Furthermore, overtwisting and its disadvantages are discussed.

A. Kinematics of TSAs

Fig. 1 shows the schematic of the kinematic model of TSAs. The axial contracted string length x is derived in [12] as

$$x = \sqrt{L_0^2 - r^2\theta^2} \tag{1}$$

where L_0 is the original string length, r is the radius of the string, and θ is motor rotation. The stroke (linear displacement) Δx can be calculated as $\Delta x = L_0 - x$.

Fig. 2 shows two kinds of twisting methods of TSAs, TSS and TLS. TSS entails the twisting of a single string, whereas TLS involves the creation of a loop with a single string and subsequently twisting it. To elaborate further, TLS encompasses the twisting of two strings arranged in parallel.

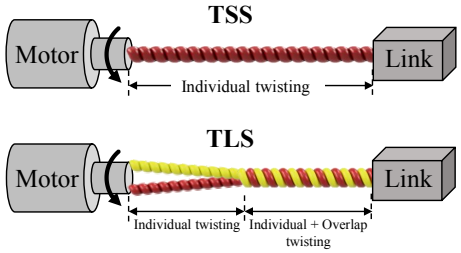

Fig. 2. Schematic representation of a twisted single string (TSS) and twisted looped single string (TLS).

These twisting methods, as outlined, cause two distinct types of twisting, namely IT and OT. IT is the self-twisting of the string, whereas OT is the mutual twisting of multiple strings. TSS exclusively encompasses IT, aligning well with the conventional kinematic model (1). In contrast, TLS, which includes both IT and OT, requires the extension of the axial contracted string lengths model resulting from both IT and OT. The distinct contributions to the axial contracted string length by IT (x_i) and the axial contracted string length by OT (x_o) were derived in [1] as

$$x_i = \sqrt{L_0^2 - r_i^2\theta_i^2} \tag{2}$$

$$x_o = \sqrt{x_i^2 - r_o^2\theta_o^2} \tag{3}$$

where r_i is the radius of IT, r_o is the radius of OT, θ_i is the IT angle, and θ_o is the OT angle. TLS (bottom figure of Fig. 2) always includes θ_i and θ_o in a one-to-one ratio (i.e., $\theta_i = \theta_o$). Moreover, the axial contracted string length by IT x_i has a role of original string length [as x_i in (3)] for OT.

B. Overtwisting and Maximum Stroke of TSAs

This subsection introduces the overtwisting of TSAs and its implication. We define the variables associated with overtwisting and maximum stroke. The stroke ratio S, representing the percentage stroke over the original string length, is defined as

$$S := \frac{\Delta x}{L_0} \times 100. \tag{4}$$

The maximum stroke ratio S_{max}, representing the percentage maximum stroke ratio before overtwisting, is defined as

$$S_{max} := \frac{\Delta x_{max}}{L_0} \times 100 \tag{5}$$

where Δx_{max} is the maximum stroke before overtwisting.

Fig. 3 shows the motor rotation vs. TLS stroke curve during the overtwisting interval. As shown in Fig. 3, when a certain amount of twist is applied to the string, exceeding approximately 30% of the stroke over the original string length, the string initiates a twisting process forming a coil; this is called overtwisting. This phenomenon intensifies hysteresis during the twisting and untwisting cycles [11]. The exacerbated hysteresis due to overtwisting not only complicates the prediction of the TSAs behavior, but also diminishes the efficiency and lifespan of TSAs [10], [11].

Fig. 4 shows the experimental results of the maximum stroke ratio S_{max} for both TSS and TLS. Notably, S_{max}

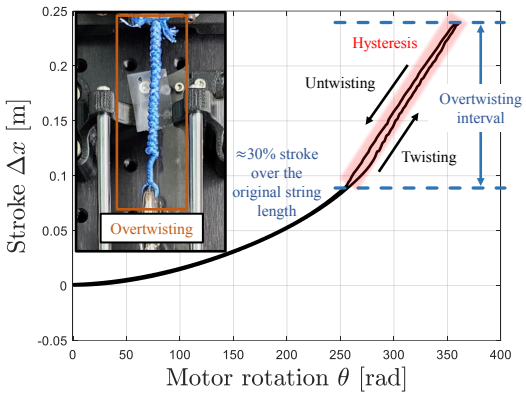

Fig. 3. Motor rotation vs. TLS stroke curve during the overtwisting interval. The overtwisting occurs at approximately 30% stroke over the original string length (i.e., $S_{max} \approx 30\%$) and causes hysteresis during twisting and untwisting cycles.

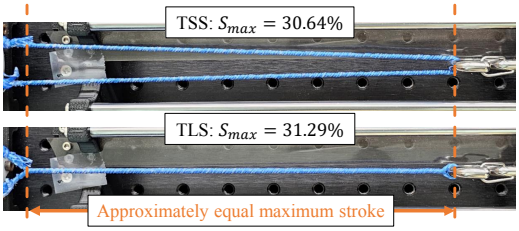

Fig. 4. Maximum stroke ratio S_{max} of TSS and TLS.

values are approximately equal despite TLS involves OT. This observation constitutes a crucial finding that forms the basis for the key concept discussed in Section III.

III. Effect of Locking on TLS

The approximately equal maximum stroke ratios of both TSS and TLS (as depicted in Fig. 4) can be attributed to the presence of a locking point generated by OT. The twisting process illustrated in Fig. 5 exemplifies how OT introduces this locking point, inhibiting the propagation of IT beyond that point. Consequently, IT accumulates nonuniformly, primarily within the interval extending from the motor to the locking point. The locking point tends to move closer to the motor as the motor rotation (twisting) intensifies, causing a reduction in the effective string length for IT. This reduction in the effective string length accelerates overtwisting because the twists accumulate in a progressively confined space.

An important observation derived from the experiments depicted in Fig. 5 is that the locking point imposes constraints on the propagation of IT, even when there is an available string length beyond this point (i.e., from the locking point to the link). This phenomenon results in an increased density of IT toward the side nearer to the motor. The maximum stroke can be expanded if this surplus string length can be used (twisted) by IT before being constrained by OT. This establishes the foundational principle of our study, aiming to enhance the maximum stroke while avoiding overtwisting by effectively leveraging the twisting potential of the string. The central idea involves harnessing the string that possess the capacity of IT within the area between the

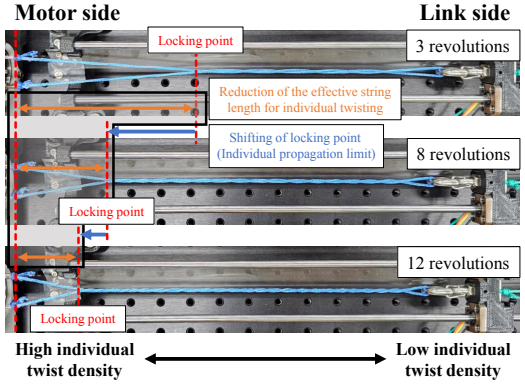

Fig. 5. Twisting behavior of TLS. OT introduces the locking point, which limits IT propagation.

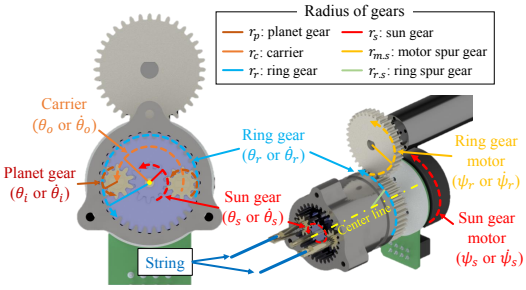

Fig. 6. Configuration of a planetary gear system for the implementation of TSA-based continuously variable transmission [13].

locking point and link to augment the maximum stroke. This concept can be facilitated by controlling the ROI.

The ROI, $C(k)$, representing the ratio between the variation in OT and IT angles, is defined as

$$C(k) := \frac{\Delta\theta_o(k)}{\Delta\theta_i(k)} \tag{6}$$

where $\Delta\theta_o(k)$ is the variation in the OT angle and $\Delta\theta_i(k)$ is the variation in the IT angle, and k denotes the sequence step. The controllability of ROI allows to realize the key idea of this study. For instance, to exploit more string segments that possess the capacity of IT before being locked by the locking point, $C(k)$ can be strategically set to a low value because it enables IT to proceed at a higher rate than OT. The controllability of the ROI can be ensured by using a TSA-based continuously variable transmission (CVT) [13]. Fig. 6 shows the configuration of the planetary gear system for implementing the TSA-based CVT. The sun gear motor (ψ_s or $\dot{\psi}_s$) directly rotates the sun gear (θ_s or $\dot{\theta}_s$); the ring gear motor (ψ_r or $\dot{\psi}_r$) rotates the ring gear (θ_r or $\dot{\theta}_r$) via spur gears. Subsequently, the sun and ring gears rotate the carrier (θ_o or $\dot{\theta}_o$) and planet gear (θ_i or $\dot{\theta}_i$), respectively. As shown in Fig. 6, the string is connected to planet gears. Therefore, θ_o and θ_i represent OT angle and IT angle, respectively. The kinematics of a planetary gear system with input $\{\dot{\psi}_s, \dot{\psi}_r\}$ and output $\{\dot{\theta}_o, \dot{\theta}_i\}$ can be derived as

$$\begin{Bmatrix} \dot{\theta}_o \\ \dot{\theta}_i \end{Bmatrix} = \begin{bmatrix} \frac{r_s}{2\,r_c} & \frac{r_r}{2\,r_c} \\ -\frac{r_s}{2\,r_p} & \frac{r_r}{2\,r_p} \end{bmatrix} \begin{bmatrix} 1 & 0 \\ 0 & -\frac{r_{m,s}}{r_{r,s}} \end{bmatrix} \begin{Bmatrix} \dot{\psi}_s \\ \dot{\psi}_r \end{Bmatrix} = J_{p.g.} \begin{Bmatrix} \dot{\psi}_s \\ \dot{\psi}_r \end{Bmatrix} \tag{7}$$

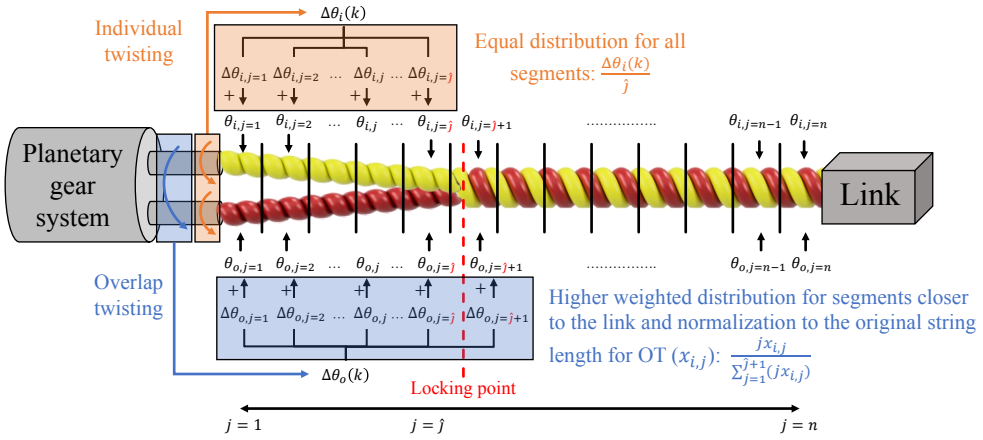

Fig. 7. Schematic representation of IT and OT propagation.

where r_p, r_s, r_c, r_r, $r_{m.s}$, and $r_{r.s}$ are the radii of planet gear, sun gear, carrier, ring gear, motor spur gear, and ring spur gear, respectively. Note that r_c and r_r can be expressed as $r_c = r_s + r_p$ and $r_r = r_s + 2r_p$, respectively. The Jacobian $J_{p.g}$ is a nonsingular matrix. Therefore, there always exists an input that satisfies any desired output, i.e., OT (θ_o) and IT (θ_i) can be arbitrarily controlled by controlling $\{\dot{\psi}_s, \dot{\psi}_r\}$.

IV. Kinematic Modeling of TSAs Accounting for Locking and ROI Optimization

With a controllable ROI, the optimal ROI trajectory, i.e., the sequence of $C(k)$ maximizing the maximum stroke ratio S_{max}, should be determined. The optimal ROI trajectory can be attained using a proper kinematic model that accurately reproduces the actual twisting behavior of TSAs. However, the conventional kinematic model (2) and (3) cannot describe the intricate twisting behavior, including the locking point. Therefore, in this section, a kinematic model of TSAs accounting for locking is proposed, and an optimization method for deriving the optimal ROI trajectory is described.

A. Kinematic Modeling of TSAs Accounting for Locking

1) Individual Propagation: Fig. 7 shows the schematic of IT propagation, where the entire TSA is divided into n-small TSAs. The segment index $j \in \mathbb{Z}^+$ specifies each segment from $j = 1$ for a neighboring segment of the planetary gear system to $j = n$ for that of the link. Suppose that a locking point exists in the $(j+1)$-th segment (which will be determined in Section IV-A.3) and the j-th segment is the last segment that allows IT propagation, then the variation in the IT angle at the k-th step, $\Delta\theta_i(k)$ is assumed to be equally distributed up to the $\hat{j}$-th segment because of locking. This equal distribution is hypothesized considering the nature of even IT propagation without locking (top figure of Fig. 4). Subsequently, the variation in the IT angle in the j-th segment at the k-th step, $\Delta\theta_{i,j}(k)$, can be expressed as

$$\Delta\theta_{i,j}(k) = \begin{cases} \frac{\Delta\theta_i(k)}{\hat{j}}, & \forall j \in [1, \hat{j}] \\ 0, & \forall j \in [\hat{j}+1, n] \end{cases}. \tag{8}$$

Assigning zero variation for all $j \in [\hat{j}+1, n]$ represents that the variation in the IT angle, $\Delta\theta_i(k)$, does not propagate from the locking point. The IT angle in the j-th segment at the k-th step, $\theta_{i,j}(k)$, propagates to the $(k+1)$-th step as

$$\theta_{i,j}(k+1) = \theta_{i,j}(k) + \Delta\theta_{i,j}(k), \ \forall j \in [1, n]. \tag{9}$$

Similar to (2), the axial contracted string length by IT in the j-th segment at the k-th step, $x_{i,j}(k)$, can be derived as

$$x_{i,j}(k) = \sqrt{L_n^2 - r_i^2\theta_{i,j}^2(k)}, \ \forall j \in [1, n] \tag{10}$$

where L_n is the original string length for IT in each segment, defined as $L_n := \frac{L_0}{n}$. IT is designed to propagate only up to the $\hat{j}$-th segment as in (8). Therefore, in (10), $x_{i,j}$ for all $j | j > \hat{j}$ remains constant.

2) Overlap Propagation: Fig. 7 shows the schematic of OT propagation. The variation in the OT angle at the k-th step, $\Delta\theta_o(k)$ is assumed to be distributed up to the $(\hat{j}+1)$-th segment in a linearly weighted manner with normalization to $x_{i,j}$ (i.e., normalization to the original string length for OT). The weighted distribution mathematically expresses the biased OT propagation as in Fig. 5 (higher OT density at the link compared to that at the motor). The normalization to $x_{i,j}$ plays a role in fair distribution among segments (i.e., the larger $x_{i,j}$ a particular segment includes, the larger OT is assigned). Subsequently, the variation in the OT angle in the j-th segment at the k-th step, $\Delta\theta_{o,j}(k)$, is expressed as

$$\Delta\theta_{o,j}(k) = \begin{cases} \Delta\theta_o(k)\frac{jx_{i,j}}{\sum_{j=1}^{\hat{j}+1}(jx_{i,j})}, & \forall j \in [1, \hat{j}+1] \\ 0, & \forall j \in [\hat{j}+2, n] \end{cases}. \tag{11}$$

Assigning zero variation for all $j \in [\hat{j}+2, n]$ represents that the variation in the OT angle, $\Delta\theta_o(k)$, does not propagate beyond the locking point. The OT angle in the j-th segment at the k-th step, $\theta_{o,j}(k)$, propagates to the $(k+1)$-th step as

$$\theta_{o,j}(k+1) = \theta_{o,j}(k) + \Delta\theta_{o,j}(k), \ \forall j \in [1, n]. \tag{12}$$

Similar to (3), the axial contracted string length by OT in the j-th segment at the k-th step, $x_{o,j}(k)$, can be derived as

$$x_{o,j}(k) = \sqrt{x_{i,j}^2(k) - r_o^2\theta_{o,j}^2(k)}, \ \forall j \in [1, n]. \tag{13}$$

OT is designed to propagate up to the $(\hat{j}+1)$-th segment as in (11). Therefore, in (13), $x_{o,j}(k)$ for all $j | j > \hat{j}+1$ remains

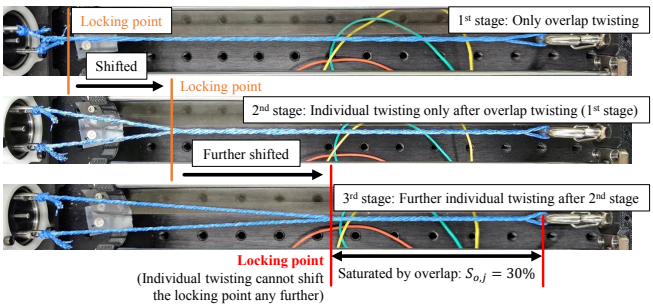

Fig. 8. Shift of the locking point.

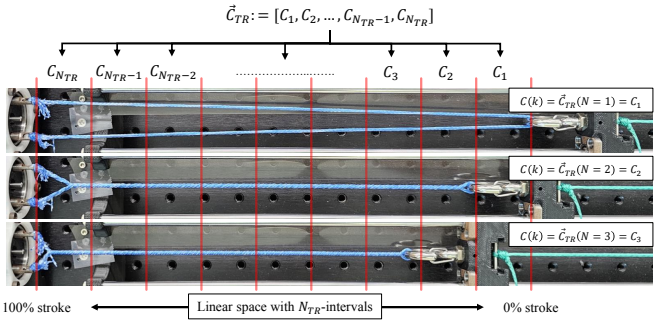

Fig. 9. Schematic representation of the setting for ROI optimization.

constant. The axial contracted string length and stroke ratio of the entire TSA at the k-th step, denoted as $x(k)$ and $S(k)$, respectively, are derived as

$$x(k) = \sum_{j=1}^{n} x_{o,j}(k) \tag{14}$$

$$S(k) = \frac{L_0 - x(k)}{L_0} \times 100 = \frac{\Delta x(k)}{L_0} \times 100. \tag{15}$$

3) Determining the Locking Point: Fig. 8 shows the shift of the locking point. In the first stage, OT (i.e., $C(k) = \infty$) produces a locking point (top figure). In the second stage, when IT (i.e., $C(k) = 0$) is applied after OT (first stage), the locking point shifts in a direction away from the motor (middle figure). In the third stage, however, this shift of the locking point ends at a certain point and IT cannot shift the locking point any further (bottom figure). The process where IT shifts the locking point is the scenario of OT accumulation toward the link. If the OT stacking continues, it will eventually end because of space constraints. Here, the segments between the locking point and link is fully occupied with the maximum amount of OT. This signifies saturation where saturation indicates that the string is just before overtwisting (i.e., $S = S_{max}$).

For the mathematical description of this analysis, the stroke ratio of IT and OT in the j-th segment at the k-th step, denoted as $S_{i,j}(k)$ and $S_{o.j}(k)$, respectively, are defined as

$$S_{i,j}(k) := \frac{L_n - x_{i,j}(k)}{L_n} \times 100 \tag{16}$$

$$S_{o,j}(k) := \frac{x_{i,j}(k) - x_{o,j}(k)}{x_{i,j}(k)} \times 100. \tag{17}$$

Because the string is typically saturated when the stroke ratio is equal to 30% (i.e., in (5), $S_{max} = 30\%$), it can be assumed that the string of each of the n-small TSAs is also saturated when the stroke ratio is equal to 30%. Under this assumption, the saturated segments by OT can be represented by $S_{o,j} = 30\%$. Thus, $\hat{j}$ can be determined as

$$\hat{j} = \max(j) - 1, \ \forall j | S_{o,j} < 30 \tag{18}$$

where $j|S_{o,j} < 30$ indicates the segments that are neither saturated nor overtwisted. The locking point is assumed to exist in the $(\hat{j}+1)$-th segment. Thus, the IT propagation limit, $\hat{j}$, can be determined by selecting the segment before the last one of the non-saturated segments, as shown in (18).

To summarize the discussion of the proposed model, IT is designed to propagate evenly up to the locking point based on the even propagation nature of IT observed in the top figure of Fig. 4. This IT propagation provides an original string length for OT $x_{i,j}$ (10), which is used by OT to generate $x_{o,j}$ (13), which in turn is used to obtain the axial contracted string length of entire TSA, x (14). The OT propagation is designed to distribute more twists to the segments closer to the link from the observed biased OT propagation shown in Fig. 5. The OT propagation with this weighted distribution is designed to saturate the string in the segments closer to the link first, i.e., this design saturates from nearer to farther away from the link in turn. Combining this sequential saturation design with the locking point determination method (18), which investigates unsaturated segments, implies that this combined model is intentionally designed such that segments closer to the link are sequentially locked by the locking point. This is the mathematical representation of the locking point moving toward the motor, as shown in Fig. 5.

B. ROI Trajectory Optimization

Fig. 9 shows the schematic representation of the setting for ROI optimization. The full range of the stroke ratio (from 0% to 100%) is divided linearly into N_{TR}-intervals. The ROI vector $\vec{C}_{TR}$, defined as $\vec{C}_{TR} := [C_1, C_2, \cdots, C_{N_{TR}-1}, C_{N_{TR}}]$, includes C_N up to $N = N_{TR}$ as its elements. Each C_N is assigned to the N-th interval in a one-to-one manner from $N = 1$ to $N = N_{TR}$. This means that when the link is in the N-th interval, C_N should be used as the ROI. For instance, as shown in Fig. 9, when the link passes through the first (top), second (middle), and third (bottom) intervals, the ROI $C(k)$ is set to C_1, C_2, and C_3, respectively. To generate the optimal ROI trajectory $\vec{C}_{opt}$, substituting $x_{i,j}$ in (13) with (10) yields

$$x_{o,j}(k) = \sqrt{L_n^2 - r_i^2\theta_{i,j}^2(k) - r_o^2\theta_{o,j}^2(k)}, \ \forall j \in [1, n]. \tag{19}$$

In (19), $\theta_{i,j}(k)$ and $\theta_{o,j}(k)$ are functions of the sequences of $\Delta\theta_{i,j}$ and $\Delta\theta_{o,j}$ from the first to the $(k-1)$-th step, as described in (9) and (12), respectively. Therefore, $x_{o,j}(k)$ can be written as $x_{o,j}(k) = x_{o,j}\left(\Delta\theta_{i,j}(1:k-1), \Delta\theta_{o,j}(1:k-1)\right)$, where $(1:k-1)$ indicates the sequence from the first to the $(k-1)$-th step. By the definition of $C(k)$ in (6), $x_{o,j}(k) = x_{o,j}\left(\Delta\theta_{i,j}(1:k-1), C(1:k-1)\right)$. With the setting in

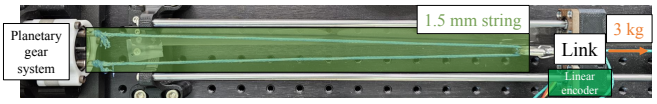

Fig. 10. Experimental setup to validate the proposed kinematic model and ROI trajectory optimization method.

Fig. 9, $C(k)$ is represented by $\vec{C}_{TR}$, yielding $x_{o,j}(k) = x_{o,j}(\Delta\theta_{i,j}(1:k-1), \vec{C}_{TR})$. Eventually, substituting this result for $x_{o,j}$ in (14) allows the axial contracted string length and stroke ratio of the entire TSA, $x(k)$ in (14) and $S(k)$ in (15), to be expressed as functions of $\vec{C}_{TR}$ as

$$x(k) = x(\vec{C}_{TR}) \tag{20}$$

$$S(k) = \frac{L_0 - x(k)}{L_0} \times 100 = S(\vec{C}_{TR}). \tag{21}$$

The optimal ROI trajectory $\vec{C}_{opt}$, which maximizes the maximum stroke ratio (21), can be obtained as a solution to the following optimization problem:

$$\begin{aligned} \vec{C}_{opt} = &\underset{\vec{C}_{TR}}{\operatorname{argmax}}\, S(\vec{C}_{TR}) \\ &\text{subject to } S_{i,j} \leq 30 \\ &\qquad 0 \leq C_N \leq 1 \end{aligned} \tag{22}$$

where the constraint $S_{i,j} \leq 30$ indicates that overtwisting by IT is not allowed during optimization. Please note that overtwisting by OT is automatically prevented by the locking point determination method (18). To force the trajectory to behave between the conventional TSS and TLS methods, C_N is bounded between zero and one.

V. Experimental Results

A. Experimental Setup and TSA-based CVT Controller Design

Before presenting the main results of this study, we provide a description of the experimental setup and the TSA-based CVT controller used in the experiments.

1) Experimental Setup: Fig. 10 shows the experimental setup to validate the proposed kinematic model and ROI trajectory optimization method. This includes a linear encoder (HEDS-9740, 360LPI) for measuring the link position, two motor controllers (ESCON 70/10), MCU (ARM Cortex-A9), a string (Dyneema SK78, LIROS) with a nominal diameter of 1.5 mm and an original length of 315 mm, a ring gear motor (120 Watt BLDC, MAXON) for ring gear rotation with a rotary encoder (2048 CPT), and a sun gear motor (60 Watt BLDC, MAXON) for sun gear rotation with a rotary encoder (1024 CPT). The radius parameters of the planetary gear (Fig. 6) used for the experiment are $\{r_s, r_p, r_{m.s}, r_{r.s}\} = \{6, 5, 18, 20\}$ mm.

2) TSA-based CVT Controller Design: Considering the primary objective of utilizing TSA-based CVT is to control $C(k)$—i.e., the independent control of $\Delta\theta_o(k)$ and $\Delta\theta_i(k)$—the angular velocity of IT, $\dot{\theta}_i(k)$ is designed to serve two purposes: position regulation and velocity control, as

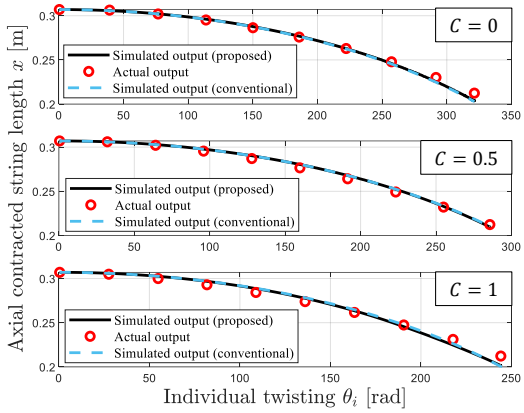

Fig. 11. Validation of the proposed model across various C values.

$$\dot{\theta}_i(k) = \begin{cases} K_p^i(\theta_{i,des}(k) - \theta_i(k)) & \text{position regulation} \\ \omega_i & \text{velocity control} \end{cases} \tag{23}$$

where K_p^i is the proportional gain of IT control, $\theta_{i,des}(k)$ is the desired value of IT, and ω_i is the constant angular velocity of IT. The position regulation control law is employed to examine the maximum stroke by gradually increasing twisting. The control law for velocity control is employed to observe the output stroke behavior under continuous twisting up to the maximum stroke, determined by the position regulation control law. The angular velocity of OT, $\dot{\theta}_o(k)$, can be designed to comply with the given $C(k)$ as

$$\begin{aligned} \Delta\theta_i(k) &= \theta_i(k) - \theta_i(k-1) \\ \Delta\theta_{o,des}(k) &= C(k)\Delta\theta_i(k) \\ \theta_{o,des}(k) &= \theta_{o,des}(k-1) + \Delta\theta_{o,des}(k) \\ \dot{\theta}_o(k) &= K_p^o(\theta_{o,des}(k) - \theta_o(k)) \end{aligned} \tag{24}$$

where K_p^o is the proportional gain of OT control. The first equation captures the variation in IT, $\Delta\theta_i(k)$. The second equation provides the variation in the desired value of OT, $\Delta\theta_{o,des}(k)$, complying with the given $C(k)$. The third equation represents that the desired value of OT, denoted as $\theta_{o,des}(k)$, should be updated with $\Delta\theta_{o,des}(k)$ provided by the second equation. The last equation is the control law for the position regulation of OT.

However, $\{\dot{\theta}_o, \dot{\theta}_i\}$ is the output of the planetary gear, whereas the actual control inputs are the angular velocities of the sun and ring gear motors. To determine the corresponding actual input $\{\dot{\psi}_s, \dot{\psi}_r\}$ to the given $\{\dot{\theta}_o, \dot{\theta}_i\}$, an explicit form can be derived by left multiplying $J_{p.g}^{-1}$ to (7).

B. Kinematic Model of TSAs Accounting for Locking

Fig. 11 validates the proposed model across various C values, $C = \{0, 0.5, 1\}$. The output represents the axial contracted string length of the entire TSA (14). The actual output, represented by the red dots, was obtained by rotating the motor with the velocity control law (23) of $\omega_i = 200$ RPM, up to a stroke ratio of 30% ($S = 30\%$). The black

TABLE I
SUMMARIZED RESULTS OF THE PROPOSED KINEMATIC MODEL VALIDATION AND RADIUS OPTIMIZATION

Model validation and radius optimization					
Metric	e^0_{rms}	$e^{0.5}_{rms}$	e^1_{rms}	$r_{i,opt}$	$r_{o,opt}$
Proposed [mm]	2.6272	2.4880	4.1765	0.7140	1.1354
Conventional [mm]	2.9545	2.5103	4.1811	0.7172	0.6277

and blue-dotted curves represent simulated output of proposed and conventional model, respectively. The simulated output of the proposed model is derived from simulating the model presented in Section IV. The required inputs for the simulation, $\Delta\theta_i(k)$ in (8) and $\Delta\theta_o(k)$ in (11), are calculated from the differences in $\theta_i(k)$ and $\theta_o(k)$ that were measured when obtaining the actual output. The number of segments was set to $n = 300$; this is a tuning parameter, and a high value can be used for high precision. In this study, the original string length of 315 mm was divided into 300 segments ($n = 300$) such that each segment had an original length of approximately 1 mm, and higher n values did not show improvement. The simulated output of the conventional model is calculated using (2) and (3), along with $\theta_i(k)$ and $\theta_o(k)$ that were measured when obtaining the actual output. Please note that during simulation, the radius parameters r_i and r_o were optimized to minimize the sum of root mean square errors between the actual and simulated outputs for all C values. The root mean square error e^*_{rms} is defined, where the superscript $*$ denotes the C value. The optimal values of radii, $r_{i,opt}$ and $r_{o,opt}$, are obtained as

$$\{r_{i,opt}, r_{o,opt}\} = \underset{\{r_i,r_o\}}{\operatorname{argmin}}(e^0_{rms} + e^{0.5}_{rms} + e^1_{rms}). \quad (25)$$

Table I summarizes the results of the proposed kinematic model validation and radius optimization. While the performance difference between the proposed and conventional models is minimal, the significance of the proposed model comes from its physical validity as reflected in the radius optimization result. Table I shows that, in the proposed model, the effective (optimized) radius of OT is larger than IT, which aligns with physical expectations. Conversely, the conventional model suggests a smaller OT radius than IT. This implies that the proposed model more accurately represents the actual physical behavior of twisting as it is designed based on observed physical phenomena like locking point. Importantly, this physically faithful design facilitates the realization of a key idea of this paper via ROI trajectory optimization.

C. ROI Trajectory Optimization

Fig. 12 shows the optimal ROI trajectory and experimental results of the proposed method. The optimal ROI trajectory was obtained using (22) with the number of segments and transmissions set to $n = 300$ and $N_{TR} = 20$, respectively, along with the optimal radius parameters from Table I. The number of transmissions N_{TR} is a tuning parameter, and a higher value provides a higher performance. In this study, we set 20 transmissions (N_{TR}) in the full range of stroke (from 0% to 100% stroke). This means that transmissions occurred at approximately 15 mm distances, and using smaller transmission distances (using higher N_{TR} value) did not improve the performance. During simulation, $\Delta\theta_i$ increased by 0.001 revolutions at each simulation step. Fig. 12(a) shows the optimized ROI trajectory. The simulation resulted in a maximum stroke ratio of 44% ($S_{max} = 44\%$) with the optimal trajectory. This implies that the right interval of the $S_{max} = 44\%$ line [black-shaded box in Fig. 12(a)] is invalid (redundant) because ROI values in this interval result from optimizing the full range of stroke intervals by dividing them into N_{TR}, instead of using the $S = 0\%$ to $S = S_{max}$ interval (because S_{max} cannot be defined prior to optimization); thus, the result of $S_{max} = 44\%$ derived from the optimization is only the result of the transmission that occurred before $S = S_{max} = 44\%$. In other words, ROI values after $S = S_{max} = 44\%$ are irrelevant to the result of $S_{max} = 44\%$. To determine the optimal ROI trajectory for the actual experiment, the valid interval (orange-shaded box) is directly used. However, the last ROI value of the valid interval ($C \approx 1$) is used for the invalid interval's subsequent stroke. The actual trajectory applied in the experiment is denoted by the red-dotted line in Fig. 12(a).

Fig. 12(b) shows the experimental results of the proposed method, obtained with the angular velocity of IT, $\omega_i = 200$ RPM (23). The optimal ROI trajectory (black curve) achieves $S_{max} = 53.44\%$, representing an improvement of approximately $23.44\%p$ over that of conventional TSAs ($S_{max} \approx 30\%$). Compared to simulation results, an additional stroke of approximately $9\%p$ is observed, which is mainly attributed to model errors arising from the intricate twisting nature of TSAs, which cannot be perfectly captured mathematically. For comparison with conventional twisting, a constant $C = 1$ trajectory is applied under identical conditions. Conventional twisting (red curve) remains non-hysteretic until the critical point, $S = 30\%$, after which it exhibits hysteresis. In contrast, the proposed method displays significantly reduced hysteresis across the entire interval. For better visibility, the green-shaded box in Fig. 12(b) is magnified in (c). The hysteresis and jittering induced by overtwisting are evident in the case of conventional twisting. Fig. 13 emphasizes the significance of the proposed method by comparing the twist shapes of the proposed and conventional twisting methods at $S \approx 53.44\%$. The bottom figure in Fig. 13 demonstrates the twist shape of conventional twisting, revealing the coiling caused by overtwisting. The observed coiling displays a uniform shape, consistent with the coiling behavior of overtwisted strings that have undergone a training process, as discussed in [11]. While uniform coiling enhances stroke consistency in the overtwisting interval [11], it necessarily introduces hysteresis during the twisting and untwisting cycles. Furthermore, the separator-based method [10] for inducing twisting in a confined space is likely to cause more indiscriminate coiling rather than uniform coiling, potentially leading to greater hysteresis compared with the uniform coiling-induced hysteresis shown in Fig. 12(c). However,

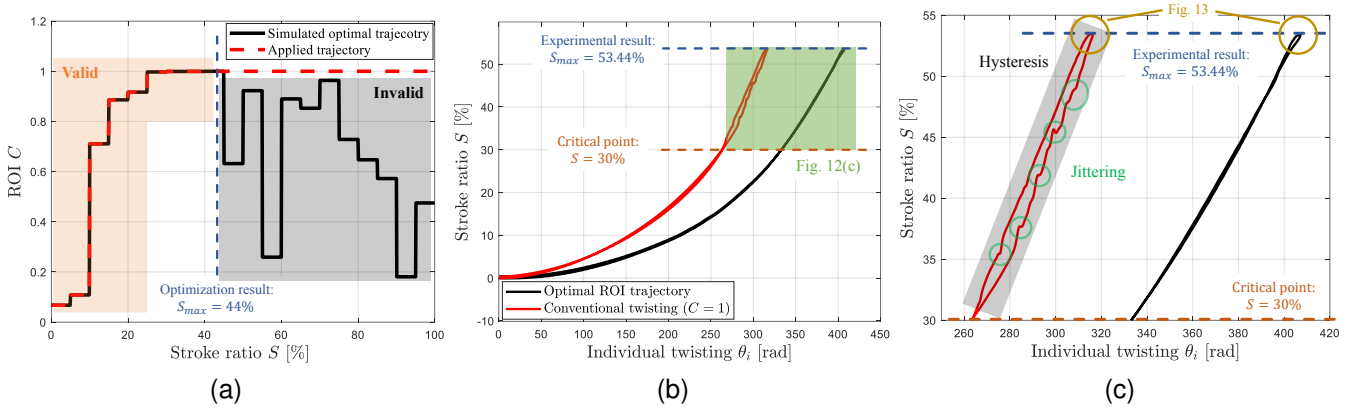

Fig. 12. Optimal ROI trajectory and experimental results of the proposed method. (a) ROI optimization result. (b) Experimental results of the proposed method. (c) Magnified view of the hysteretic interval in the experimental results.

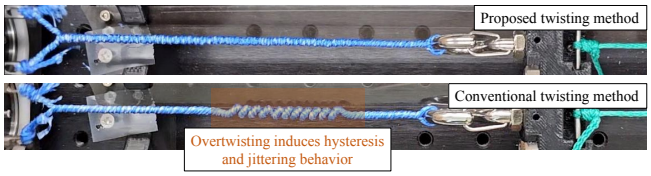

Fig. 13. Comparison image of the twist shape between the proposed twisting method (top) and conventional twisting method (bottom) at $S \approx 53.44\%$.

the top figure in Fig. 13 shows that the twist shape of the proposed method does not exhibit overtwisting (coiling), resulting in hysteresis-free performance.

VI. Conclusion

This study introduced an innovative approach to enhance the maximum stroke of TSAs by adjusting the ROI. The key insight was the observation that the maximum stroke of the TLS, which includes both IT and OT, is approximately equal to that of the TSS, which only includes IT. This result is attributed to the locking point introduced by OT in TLS. The proposed method strategically employed a controllable ROI to effectively use string segments that possess the capacity of IT before being locked by OT. To facilitate this, a kinematic model of TSAs accounting for the locking, was developed, and it successfully reproduced the actual behavior of TSAs under various ROIs. The optimization process using this model yielded an optimal ROI trajectory that maximizes the maximum stroke. Implementing the optimal ROI trajectory to the actual system achieved a maximum stroke ratio of 53.44%, surpassing the conventional limitation of 30%. Crucially, this enhancement was accomplished without introducing overtwisting, thus avoiding hysteresis and oscillatory behavior.

Despite these accomplishments, several areas should be addressed in future research. A primary limitation lies in the use of two motors for controllable ROI, leading to an increase in the system size. Hence, exploring single-motor-based methods for achieving an extended maximum stroke would enhance the practicality of the proposed approach. Additionally, the proposed twisting method with a variable ROI requires a motor torque profile different from that of conventional twisting methods with a constant ROI. Analyzing the required torque profile for the proposed twisting method, both theoretically and experimentally, and using these findings to select appropriate motors and optimize the planetary gear design could enhance system efficiency.

References

[1] S. H. Jeong *et al.*, "Designing anthropomorphic robot hand with active dual-mode twisted string actuation mechanism and tiny tension sensors," *IEEE Robot. Autom. Lett.*, vol. 2, no. 3, pp. 1571–1578, 2017.

[2] M. Tavakoli, R. Batista, and L. Sgrigna, "The uc softhand: Light weight adaptive bionic hand with a compact twisted string actuation system," in *Actuators*, vol. 5, no. 1. MDPI, 2015, p. 1.

[3] F. Lotti *et al.*, "Development of ub hand 3: Early results," in *Proc. IEEE Int. Conf. Robot. Automat.*, 2005, pp. 4488–4493.

[4] M. Hosseini, R. Meattini, G. Palli, C. Melchiorri *et al.*, "A wearable robotic device based on twisted string actuation for rehabilitation and assistive applications," *Journal of Robotics*, vol. 2017, 2017.

[5] T. Tsabedze *et al.*, "A compact, compliant, and biomimetic robotic assistive glove driven by twisted string actuators," *International Journal of Intelligent Robotics and Applications*, vol. 5, pp. 381–394, 2021.

[6] D. Schlesiger, G. A. Giacoppo, M. B. Schäfer, and P. P. Pott, "Twisted string actuation with position feedback for robotic endoscopy," *Current Directions in Biomedical Engineering*, vol. 7, no. 2, pp. 343–346, 2021.

[7] Q. H. Van and M. Harders, "Augmenting contact stiffness in passive haptics—preliminary results with twisted string actuation," in *2017 IEEE World Haptics Conference (WHC)*. IEEE, 2017, pp. 148–153.

[8] M. Hosseini *et al.*, "Exoten-glove: A force-feedback haptic glove based on twisted string actuation system," in *2018 27th IEEE Int. Symposium on Robot and Human Interactive Communication*, 2018, pp. 320–327.

[9] V. Skvortsova *et al.*, "Design, characterisation and validation of a haptic interface based on twisted string actuation," *Frontiers in Robotics and AI*, vol. 9, p. 977367, 2022.

[10] M. Tavakoli, R. Batista, and P. Neto, "A compact two-phase twisted string actuation system: Modeling and validation," *Mechanism and Machine Theory*, vol. 101, pp. 23–35, 2016.

[11] R. Konda *et al.*, "Overtwisting and coiling highly enhance strain generation of twisted string actuators," *Soft Robotics*, 2023.

[12] D. Popov *et al.*, "A study on twisted string actuation systems: Mathematical model and its experimental evaluation," in *2012 IEEE/RSJ Int. Conf. on Intell. Robots and Syst.* IEEE, 2012, pp. 1245–1250.

[13] J. Jang *et al.*, "Active-type continuously variable transmission system based on a twisted string actuator," *IEEE Robot. Autom. Lett.*, vol. 7, no. 2, pp. 2605–2612, 2022.